Preparation and properties of Tm-doped SiO2 -ZrO2 phase separated optical fibers for use in fiber lasers

Petr Vařák, Jan Mrázek, Wilfried Blanc, Jan Aubrecht, Michal Kamrádek, Ondřej Podrazký

Preparation and properties of Tm-doped SiO_2-ZrO_2 phase separated optical fibers for use in fiber lasers

PETR VAŘÁK,[1,*] JAN MRÁZEK,[1] WILFRIED BLANC,[2] JAN AUBRECHT,[1] MICHAL KAMRÁDEK,[1] AND ONDŘEJ PODRAZKÝ[1]

[1]*The Institute of Photonics and Electronics of the Czech Academy of Sciences, Chaberská 1014/57, 182 51 Prague, Czech Republic*
[2]*Université Côte d'Azur, Institut de Physique de Nice (INPHYNI), CNRS UMR7010, Parc Valrose, 06108 Nice, France*
[*]*varak@ufe.cz*

Abstract: Zirconium oxide (ZrO_2) is a perspective co-dopant of rare-earth ions in silica fibers for use in fiber lasers. ZrO_2 nanoparticles increase the solubility of rare-earth ions and enhance their luminescence properties. In this paper, we report on the fabrication of Zr-Tm codoped silica fibers using the MCVD method combined with modified solution-doping technique. Several fibers with different dopant concentrations were prepared and their optical properties were studied. It was found that increasing Zr concentration leads to the creation of larger ZrO_2 nanoparticles which causes unwanted attenuation. Optimal Zr concentration was found to be 1 at. %. The fiber with optimal Zr concentration and Tm concentration of 260 ppm exhibited 1.8 µm fluorescence lifetime of 420 ± 10 µs. For the first time in literature, we have demonstrated laser operation in a Zr/Tm-codoped silica fiber. The threshold for laser operation was determined to be 233 mW and the slope efficiency of 72.7% was achieved. MCVD combined with modified solution doping proved to be a feasible method of preparation of Tm-doped SiO_2-ZrO_2 optical fibers for use in fiber lasers.

1. Introduction

Thulium-doped fiber lasers operating in the 2 µm region receive growing attention nowadays for their potential in so called "eye-safe" applications such as laser surgery, biological imaging, atmospheric sensing or material processing [1-3]. Amongst materials for the fabrication of rare-earth-doped fibers, silica glass remains frequently used thanks to numerous advantages such as transparency up to NIR region, good thermal or chemical stability and high durability. Low price and good compatibility with common optical components also play a significant role in practical applications. However, several drawbacks put silica glass in disadvantage compared to other glass systems such as germanate, telluride or fluoride glass. Limited solubility of rare-earth ions in silica glass leads to the formation of clusters which causes concentration quenching and hinders luminescence properties. Silica glass also has a high phonon energy (≈1100 cm^{-1}) which increases the probability of non-radiative transitions and further limits radiative properties.

To overcome these shortcomings, silica glass needs to be modified with other oxides, i.e. Al_2O_3, P_2O_5 or Sb_2O_3 [4]. Previous studies have shown that zirconium oxide (ZrO_2) is a very perspective co-dopant of rare-earth ions in silica glass [5,6]. With an appropriate heat treatment, a phase separation can be induced in the binary SiO_2-ZrO_2 system which leads to the formation of ZrO_2 nanoparticles [7]. The presence of these nanoparticles prevents the clustering of rare-earth ions and improves luminescence properties. The zirconia particles also possess low phonon energy (≈470 cm^{-1}) which increases the number and probability of radiative transitions of rare-earth ions [8]. Furthermore, thanks to a good optical transparency, chemical durability and

high refractive index, ZrO_2 appears as a suitable candidate for the fabrication of rare-earth doped optical fibers [5].

In this paper, we report on the experimental preparation and characterization of Tm-doped SiO_2-ZrO_2 fibers. Multiple fibers with various concentrations of zirconium and thulium in the fiber core were prepared by a modified solution doping method in order to study the effect of zirconia on the photoluminescence properties of Tm^{3+} ions and to find the optimal zirconia concentration. The fiber with the best optical properties was measured in a fiber laser setup and its laser characteristics were evaluated.

2. Experimental

2.1. Preparation of sols and optical fibers

Sols with varying concentrations of zirconium and thulium were prepared, using propan-1-ol (Lachema, p.a.), ethanol (Sigma Aldrich, 96% vol.), zirconium(IV)-butoxide (Ventron GMBG, p.a.) and thulium nitrate pentahydrate (Alfa Aeasar, 99.9%). Four sols were prepared, with zirconium concentrations of 0.16 mol.dm^{-3}, 0.1 mol.dm^{-3}, 0.09 mol.dm^{-3} and 0.07 mol.dm^{-3} and thulium molar concentrations corresponding to 3% of zirconium concentration in each respective solution. The process of preparation was as follows: 9.1 g of zirconium(IV) tert-butoxide and 0.23 g of thulium nitrate pentahydrate were dispersed in 200 ml of propan-1-ol and 3.7 ml of 96% ethanol. The volume of ethanol was calculated to achieve a H_2O/Zr-butoxide ratio of 0.5. The zirconium(IV) tert-butoxide was hydrolyzed by heating at 130 °C for 18 hours. The hydrolyzed sol was partially evaporated at a rotary evaporator to reduce its volume and reach a zirconium concentration of 0.16 mol.dm^{-3}. The less concentrated sols were prepared by diluting the 0.16M sol with propan-1-ol.

The preforms were prepared by a modified chemical vapor deposition (MCVD) method [9] combined with a modified solution-doping technique [10]. A set of porous silica layers was deposited onto the inner side of pure silica tubes (F300, Heraeus) with 18 mm outer diameter and 1.4 mm wall thickness. The porous layers were soaked with the prepared sols and left to dry on air for 24 h. The soaked tubes were further dried by oxygen for 3 h, sintered and collapsed into preforms.

Optical fibers were drawn at a 6 m high drawing tower of our own construction, equipped with a graphite resistance furnace. The fibers had cladding diameter of approx. 125 µm and core diameter of approx. 10 µm. The fibers were coated during drawing with UV-curable acrylate (Desolite 3473-3-14, DSM Netherlands).

2.2. Preforms and fibers characterization methods

A Photon Kinetics A2600 refractive index profiler was used to measure the refractive index profile (RIP) of the preforms. To verify the longitudinal homogeneity of the preforms, RIPs at several longitudinal positions under nine angle projections were measured. Numerical aperture of the fibers was calculated by the Eq. (1) [11]:

$$NA = \sqrt{n_{core}^2 - n_{cladding}^2} \tag{1}$$

where n_{CORE} is the refractive index of the core and $n_{CLADDING}$ is the refractive index of the silica cladding which is equal to 1.457.

Preform samples approx. 5 mm thick were cut and polished. The dopant concentrations were measured by electron probe microanalysis (EPMA) using Cameca SX-100 at approx. 20 points across the core.

SEM images of the preform core were taken using JEOL 7000F scanning electron microscope with acceleration voltage of 15 kV.

Absorption spectra were measured using a tungsten halogen lamp as a source and a Nicolet 8700 FTIR spectrometer (with resolution of 16 cm^{-1}) in the range from 1000 nm to 2200 nm. Standard cut-back method using Ando AQ1425 optical spectrum analyzer was used to determine the minimum of background losses.

The emission spectra were measured on Nicolet 8700 spectrometer in a setup with ThorLabs FPL1054S diode as a source at 1619 nm, an optical isolator, and a wideband coupler. The spectra were measured in the range of 1700–2300 nm with 8 cm^{-1} resolution. The spectra were corrected on the insertion loss of the wideband coupler and the spectral response of the InGaAs detector.

Time-resolved luminescence was measured in a side detection setup with excitation at 1619 nm, using ThorLabs FPL1054S diode as the source and Hamamatsu InGaAs photodiode G12183-10K as the detector. The decay curves at various pump powers were normalized, and fitted by single and double exponential functions to analyze the decay characteristics and retrieve fluorescence lifetime values, which were subsequently extrapolated to zero pump power to eradicate the influence of amplified spontaneous emission (ASE) and other effects dependent on the concentration of Tm^{3+} ions, such as cross-relaxation [12].

Laser performance was measured in a laser setup depicted in Fig. 1. An in-house built erbium/ytterbium-doped fiber laser in a ring arrangement emitting at 1565 nm was used as a pumping source. The maximum pump power was limited at 0.9 W. The performance of thulium-doped fiber (TDF) was tested in a Fabry-Perot configuration in a cavity formed by high reflectivity fiber Bragg grating (HR) at 1950 nm (R~99,5%) and perpendicularly cleaved fiber end (R~3,5%). The laser spectrum was measured with a Miriad S3 spectrometer (spectral resolution 2 nm)

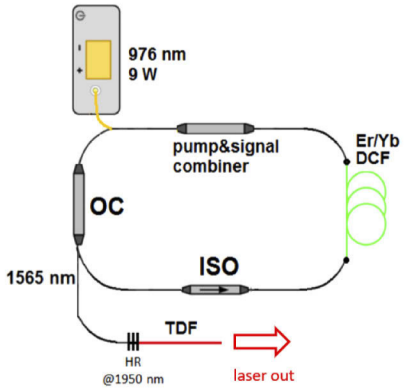

Fig. 1. Laser setup for the measurement of laser characteristics.

3. Results and discussion

The prepared preforms were characterized with respect to the dopant concentrations and refractive index differences between optical fiber cores and claddings. The results are summarized in Table 1:

Refractive index differences, numerical apertures, and dopant concentrations in the preforms increased gradually with dopant concentrations in the solutions. Refractive index profile and corresponding dopant concentration profiles of the 0.07M preform are shown in Fig. 2(a) for illustration. Other preforms displayed similar shapes of the profiles. The distributions of dopants were sufficiently homogenous across the preforms cores, the refractive index profiles followed the distributions of dopants. Refractive index and zirconium concentration data for all prepared preforms were compiled together and the resulting dependency of refractive index on zirconium

Table 1. Basic characteristics of the prepared preforms

c(Zr) in solution	Δn ($.10^{-2}$)	NA (-)	c(Zr) (at. %)	c(Tm) (ppm)
0.16 M	2.13	0,2500	1.546	480
0.10 M	1.54	0,2124	1.171	350
0.09 M	1.51	0,2103	1.044	300
0.07 M	1.23	0,1897	1.018	260

concentration is shown in Fig. 2(b). As can be seen, the data show a clear linear dependency. The scattering of the data is caused by the error of measurement of the Photon Kinetics A2600 profiler (described in detail in [13]). Due to the high refractive index of ZrO_2, the refractive index difference was higher than in Al_2O_3 doped silica fibers of comparable concentrations [14].

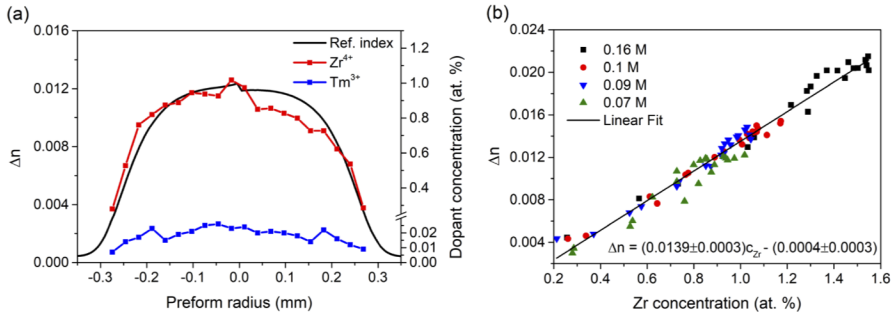

Fig. 2. a) Refractive index and concentration profiles of the 0.07M preform; b) Dependency of refractive index on the zirconium concentration calculated from the experimental data.

The presence of ZrO_2 nanoparticles in the amorphous matrix of the preforms was confirmed by SEM imaging. As can be seen in Fig. 3, the size of the nanoparticles was greatly dependent on the concentration of zirconia. In the highest doped 0.16M fiber, ZrO_2 formed large nanoparticles

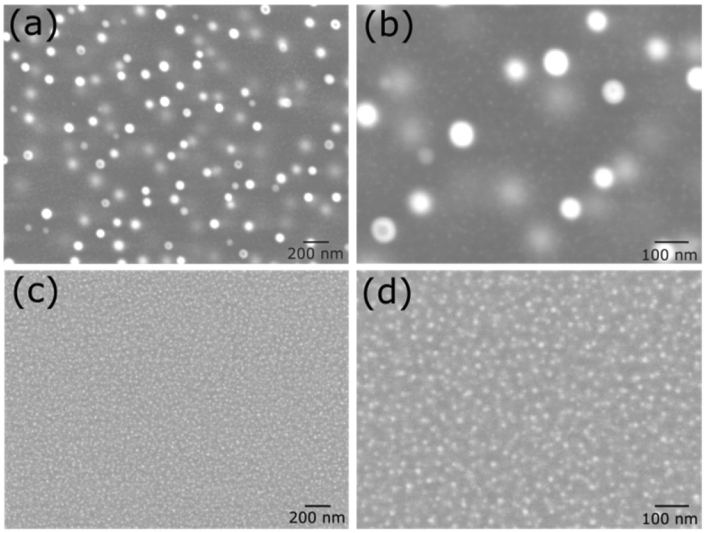

Fig. 3. SEM visualization of ZrO_2 nanoparticles, a) 0.16M preform, overall view, b) 0.16M preform, detail, c) 0.07M preform, overall view, d) 0.07M preform, detail.

with size up to 50 nm in diameter. Due to the presence of large nanoparticles, the core of the 0.16M preform exhibited a dense white coloration. On the other hand, the lowest doped 0.07M preform contained high density of small nanoparticles with diameter up to 10 nm and the preform core was transparent.

Absorption spectra of the prepared fibers are shown in Fig. 4. Optical properties of the fibers are greatly dependent on the size of the nanoparticles. In general, the attenuation of the fibers can be divided into two main components – background (intrinsic) losses and extrinsic attenuation caused by optically active dopants such as Tm^{3+} ions or OH-groups [15]. Basic optical attenuation arises from structural imperfections and density fluctuations in the matrix which are caused by the presence of nanoparticles. The Rayleigh scattering on the incorporated particles is one of the primary sources of attenuation in nanoparticle doped fibers and increases with the size of the nanoparticles and refractive index difference between host matrix and nanoparticles. The effect of nanoparticle size on the attenuation is clearly seen from the absorption spectra. The attenuation of the highest doped 0.16M fiber with largest nanoparticles could not be measured due to the extreme attenuation and impermeability of the fiber. In the other fibers, the Rayleigh scattering losses gradually diminished with decreasing concentration of zirconium and were the lowest in the 0.07M fiber with small nanoparticles.

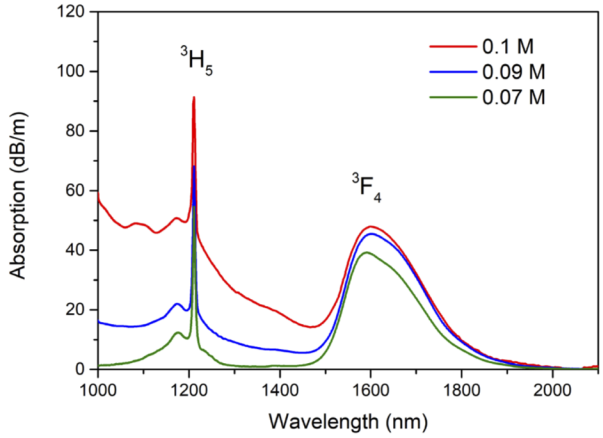

Fig. 4. Measured absorption spectra of the 0.1M, 0.09M and 0.07M fibers.

The extrinsic losses are caused mainly by optically active dopants such as rare-earth ions or OH-groups. The optical attenuation caused by Tm^{3+} ions corresponds to their absorption. Two absorption bands assigned to Tm^{3+} ions were present in the spectra – $^3H_5$ (1211 nm) and $^3F_4$ (1592 nm for 0.07M fiber). The maximum of the $^3F_4$ absorption band was slightly red-shifted for the 0.09M and 0.10M samples due to the overlap with Rayleigh scattering.

A higher limit estimate of the background losses in the 0.07M fiber was determined from the absorption spectrum at 1330 nm and was 0.9 dB/m. Standard cut-back method was used to find a minimum of background losses, which was determined to be 0.098 dB/m at 935 nm. The background losses of fibers doped with rare-earth ions are usually in the range of 0.05–0.5 dB/m [16]. The higher than usual losses in the 0.07M fiber are most likely caused by the presence of nanoparticles, i.e. high refractive index difference between nanoparticles and host matrix, or OH-impurities originating from the initial solutions.

The 0.07M fiber exhibited highest quality and lowest losses and was therefore selected for measurement of photoluminescence properties and laser performance. The luminescence properties were measured using 1619 nm diode as an excitation. The emission spectrum of the $^3F_4 \leftrightarrow {}^3H_6$ transition recorded on Nicolet 8700 spectrometer is shown in Fig. 5. The emission

spectra had the maximum at 1779 nm, the spectral shape corresponds well to thulium spectra reported elsewhere in literature [12,17].

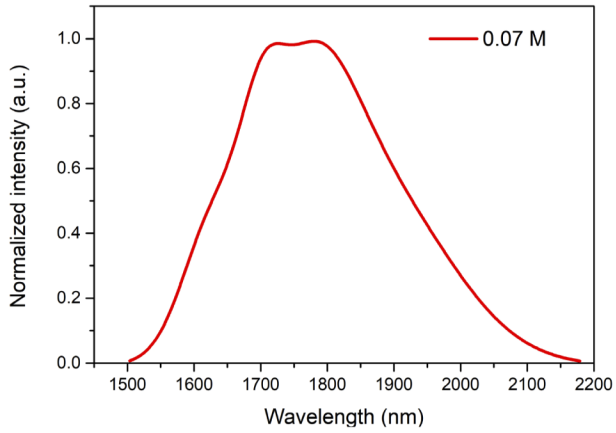

Fig. 5. Measured emission spectrum of the 0.07M fiber

Luminescence decay of the $^3F_4 \leftrightarrow {}^3H_6$ emission band was measured in a side detection setup in order to suppress the influence of amplified spontaneous emission (ASE) [12]. An example of a fluorescence decay curve for 16 mW input power is shown in Fig. 6(a). As can be seen, the fluorescence decay exhibited a significant deviation from single exponentiality. The decay curve was accurately fitted by double exponential function (adjusted R-squared = 0.99997) which returned the values of $\tau_{SLOW} = 600 \pm 1$ µs and $\tau_{FAST} = 222 \pm 1$ µs. Deviations from single exponential decay have been previously reported numerous times for Tm^{3+} ions [18,19] and have been generally attributed to several phenomena. First explanation would be inter-ionic energy transfer processes such as cross relaxation or pair-induced quenching. These processes are observed mainly in high Tm^{3+}-doped fibers because the probability of inter-ionic energy transfer increases with the decreasing distance between Tm^{3+} ions and the formation of clusters. In the case of the 0.07M fiber, low Tm^{3+} concentration of 260 ppm and the presence of ZrO_2 nanoparticles should be beneficial in terms of suppressing the clustering of Tm^{3+} ions, however Simpson et al [20] have previously shown that energy transfers resulting from the formation of clusters may occur even in Al_2O_3 co-doped silica fibers with Tm^{3+} concentrations as low as 200 ppm. Moreover, the value of 260 ppm represents the overall concentration of Tm^{3+} in the fiber, but the local concentration in the nanoparticles can be higher. Therefore, the effects of Tm^{3+}-Tm^{3+} energy transfer cannot be ruled out.

Another factor to consider is possible location of Tm^{3+} ions in different optically active sites in the matrix as suggested by Moulton et al [21] for Al_2O_3 doped silica fibers. It has been reported that rare-earth ions are preferentially partitioned in the silica-poor phase (nanoparticles) during phase separation [22]. However, Tm^{3+} ions can generally be located in a Zr-rich (ZrO_2 nanoparticles) or Zr-poor (silica matrix) environment with both sites displaying different decay rates which may cause deviations from single exponentiality. Tm^{3+} ions dispersed in an environment with higher phonon energy (silica matrix) would manifest faster decay (characterized by τ_{FAST}) than Tm^{3+} ions embedded in the ZrO_2 nanoparticles (characterized by τ_{SLOW}).

The decay curves were measured for multiple input powers and fitted by double exponential functions. The values of slow and fast components of the luminescence lifetime were extrapolated to zero pump power, which returned the values of $\tau_{SLOW} = 686 \pm 1$ µs and $\tau_{FAST} = 304 \pm 1$ µs, as shown in Fig. 6(b). Despite lower accuracy, the decay curves were fitted by single exponential function to compare the luminescence decay of the 0.07M fiber with literature, which returned

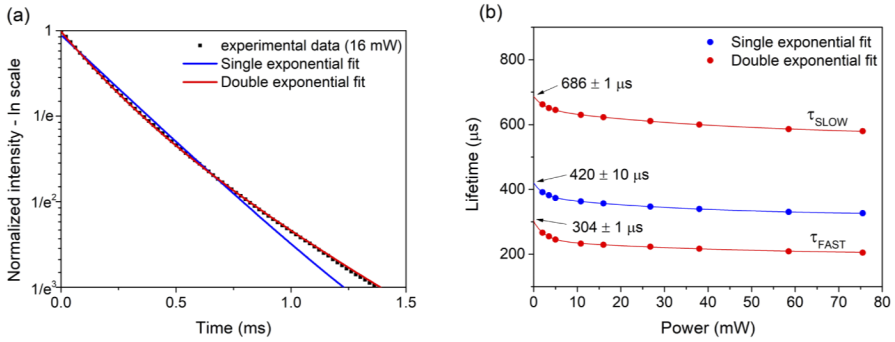

Fig. 6. a) measured decay curve of the 0.07M fiber under 16 mW excitation with single and double exponential fits, b) fluorescence lifetimes of the 0.07M fiber from single and double exponential fits of the decay curves as a function of excitation power.

the lifetime value of 420 ± 10 μs after extrapolation to zero pump power. This value corresponds well to the higher end of fluorescence lifetimes found in silica glass which usually vary between 220 and 420 μs depending on the Tm^{3+} concentration [23,24].

The 0.07M fiber was further tested as a gain medium in a fiber laser. Er/Yb-doped fiber laser emitting at 1565 nm was used as a pump source. The fiber was spliced into the laser setup and the dependence of the laser output power (P^{out}) on the absorbed pump power ($P^{abs.\ pump}$) was measured. Two main parameters were obtained: laser threshold, calculated as the intercept of the linear fit from the dependence of laser output power on absorbed pump power, and slope efficiency, a characteristic parameter that is defined by Eq. (2):

$$\eta = \frac{dP^{out}}{dP^{abs.\ pump}} \tag{2}$$

Tested fiber was gradually shortened so that several lengths of the fiber were tested. As can be seen from Fig. 7(a), optimal values of laser threshold and slope efficiency were found for the length of 1.8 m. Laser characteristics of fiber lengths below 1.8 m sharply deteriorated due to inefficient absorption of pump power. Laser data for the 1.8 m length are depicted in Fig. 7(b). The laser spectrum was centered at 1950 nm in accordance with used HR fiber Bragg grating (with respect to the spectrometer resolution). The laser threshold was 233 mW which is in good agreement with values reported in Al_2O_3 co-doped silica glass [12]. The relatively low value

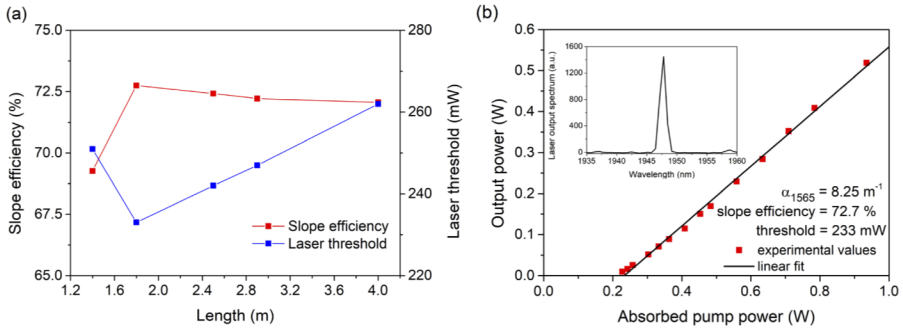

Fig. 7. a) Slope efficiency and laser threshold as functions of active fiber length, b) Output power of TDFL using 0.07M fiber (1.8 m) as a function of absorbed pump power; laser spectrum at 530 mW output power as inset

of laser threshold can be ascribed to low concentration of Tm^{3+} ions and the presence of ZrO_2 nanoparticles, since unwanted energy transfer processes, which negatively affect the threshold for laser performance, become more probable with decreasing inter-ionic distance and formation of clusters [25]. In case of slope efficiency, the low concentration of Tm^{3+} ions in the 0.07M fiber limits the choice of pump wavelengths to in-band pumping to the $^3F_4$ level. The theoretical limit of slope efficiency for 793 nm pump ($^3H_4$ level) is around 40%. Higher slope efficiencies, theoretically up to 80%, are possible to achieve only in fibers doped with high concentrations of Tm^{3+} ions with the use of so called "two-for-one" cross relaxation effect [2]. In case of in-band pumping scheme at 1565 nm, the theoretical limit has been calculated as 84% [26]. The value of slope efficiency of the 0.07M fiber was 72.7% which corresponds to 87% of the maximal theoretical value.

4. Conclusions

Tm-doped SiO_2-ZrO_2 fibers were prepared using the MCVD method combined with modified solution-doping technique. ZrO_2 nanoparticles were formed during the preform processing, their size was dependent on the Zr concentration. Optimal Zr concentration was found to be approx. 1 at. %. Silica fiber doped with 1 at. % of zirconium and 260 ppm of thulium had sufficiently low background losses and exhibited strong emission around 1.8 μm. Lifetime of the $^3F_4 \leftrightarrow {}^3H_6$ transition of Tm^{3+} ions extrapolated to zero pump power was 420 ± 10 μs. For the first time in literature, we have demonstrated laser operation in a Zr/Tm-codoped silica fiber. In a fiber laser setup, the fiber had a threshold for laser operation of 233 mW and a slope efficiency of 72.7%. MCVD combined with modified solution doping proved to be a feasible method of preparation for Tm-doped SiO_2-ZrO_2 optical fibers for use in fiber lasers.

Funding

Grantová Agentura České Republiky (19-03141S); Centre National de la Recherche Scientifique.

Disclosures

The authors declare that there are no conflicts of interest related to this article

References

1. M. N. Zervas, "High Power Fiber Lasers: A Review," IEEE J. Sel. Top. Quantum Electron. **20**(5), 219–241 (2014).
2. A. Sincore, J. D. Bradford, J. Cook, L. Shah, and M. C. Richardson, "High average power thulium-doped silica fiber lasers: review of systems and concepts," IEEE J. Sel. Top. Quantum Electron. **24**(3), 1–8 (2018).
3. M. Koska, P. Peterka, J. Aubrecht, O. Podrazky, F. Todorov, M. Becker, Y. Baravets, P. Honzatko, and I. Kasik, "Enhanced pump absorption efficiency in coiled and twisted double-clad thulium-doped fibers," Opt. Express **24**(1), 102–107 (2016).
4. I. Kasik, P. Peterka, J. Mrazek, and P. Honzatko, "Silica Optical Fibers Doped with Nanoparticles for Fiber Lasers and Broadband Sources," Curr. Nanosci. **12**(3), 277–290 (2016).
5. G. Brasse, C. Restoin, J.-L. Auguste, S. Hautreux, J.-M. Blondy, A. lecomte, F. Sandoz, and C. Pedrido, "Nanoscaled optical fibre obtained by the sol–gel process in the SiO2–ZrO2 system doped with rare earth ions," Opt. Mater. **31**(5), 765–768 (2009).
6. A. Dhar, I. Kasik, O. Podrazky, and V. Matejec, "Preparation and Properties of Er-Doped ZrO2 Nanocrystalline Phase-Separated Preforms of Optical Fibers by MCVD Process," Int. J. Appl. Ceram. Technol. **9**(2), 341–348 (2012).
7. A. Gaudon, F. Lallet, A. Boulle, A. Lecomte, B. Soulestin, R. Guinebretiére, and A. Dauger, "From amorphous phase separations to nanostructured materialsin sol–gel derived ZrO2:Eu3+/SiO2and ZnO/SiO2composites," J. Non-Cryst. Solids **352**(21-22), 2152–2158 (2006).
8. T. López-Luke, E. De La Rosa, D. Sólis, P. Salas, C. Angeles-Chavez, A. Montoya, L. A. Díaz-Torres, and S. Bribiesca, "Effect of the CTAB concentration on the upconversion emissionof ZrO2:Er3 + nanocrystals," Opt. Mater. **29**(1), 31–37 (2006).
9. S. R. Nagel, J. B. McChesney, and K. L. Walker, "An overview of the MCVDprocess and performance," IEEE J. Quantum Electron. **18**(4), 459–476 (1982).
10. J. E. Townsend, S. B. Poole, and D. N. Payne, "Solution doping technique for fabrication of rare-earth doped optical fibers," Electron. Lett. **23**(7), 329–331 (1987).

11. M. Pokhrel, G. A. Kumar, P. Samuel, K. I. Ueda, T. Yanagitani, H. Yagi, and D. K. Sardar, "Infrared and upconversion spectroscopic studies of high Er3+content transparent YAG ceramic," Opt. Mater. Express **1**(7), 1272–1285 (2011).
12. J. Cajzl, P. Peterka, M. Kowalczyk, J. Tarka, G. Sobon, J. Sotor, J. Aubrecht, P. Honzatko, and I. Kasik, "Thulium-doped silica fibers with enhanced fluorescence lifetime and their application in ultrafast fiber lasers," Fibers **6**(3), 66 (2018).
13. J. Probostova, J. Slanicka, J. Mrazek, O. Podrazky, A. Benda, and P. Peterka, "Measurement of refractive index profile of non-symmetric, complex silica preforms with high refractive index differences," Proc. SPIE **9886**, 98861G (2016).
14. M. Kamradek, I. Kasik, J. Aubrecht, J. Mrazek, O. Podrazky, J. Cajzl, P. Varak, V. Kubecek, P. Peterka, and P. Honzatko, "Nanoparticle and solution doping for efficient holmium fiber lasers," IEEE Photonics J. **11**(5), 1–10 (2019).
15. J. M. Senior, *Optical Fiber Communications: Principles and Practice*. Prentice Hall International (UK) Ltd.: London, UK, 1992.
16. J. Mrazek, I. Kasik, L. Prochazkova, V. Cuba, V. Girman, V. Puchy, W. Blanc, P. Peterka, J. Aubrecht, J. Cajzl, and O. Podrazky, "YAG ceramic nanocrystals implementation into MCVD technology of active optical fibers," Appl. Sci. **8**(5), 833 (2018).
17. A. V. Smith and J. J. Smith, "Mode instability thresholds for Tm-doped fiber amplifiers pumped at 790 nm," Opt. Express **24**(2), 975–992 (2016).
18. W. Blanc, T. L. Sebastian, B. Dussardier, C. Michel, B. Faure, M. Ude, and G. Monnom, "Thulium environment in a silica doped optical fibre," J. Non-Cryst. Solids **354**(2-9), 435–439 (2008).
19. G. Turri, V. Sudesh, M. Richardson, M. Bass, A. Toncelli, and M. Tonelli, "Temperature-dependent spectroscopic properties of in germanate, silica, and phosphate glasses: A comparative study," J. Appl. Phys. **103**(9), 093104 (2008).
20. D. A. Simpson, G. W. Baxter, S. F. Collins, W. E. K. Gibbs, W. Blanc, B. Dussardier, and G. Monnom, "Energy transfer up-conversion in Tm3+-doped silica fiber," J. Non-Cryst. Solids **352**(2), 136–141 (2006).
21. P. F. Moulton, G. A. Rines, E. V. Slobodtchikov, K. F. Wall, G. Frith, B. Samson, and A. L. G. Carter, "Tm-Doped Fiber Lasers: Fundamentals and Power Scaling," IEEE J. Sel. Top. Quantum Electron. **15**(1), 85–92 (2009).
22. W. Blanc, I. Martin, H. Francois-Saint-Cyr, X. Bidault, S. Chaussedent, C. Hombourger, S. Lacommne, P. Le Coustumer, D. Neuville, D. Larson, T. Prosa, and C. Guillermier, "Compositional Changes at the Early Stages of Nanoparticles Growth in Glasses," J. Phys. Chem. C **123**(47), 29008–29014 (2019).
23. B. M. Walsh and N. P. Barnes, "Comparison of Tm:ZBLAN and Tm: silica fiber lasers; Spectroscopy and tunable pulsed laser operation around 1.9 μm," Appl. Phys. B **78**(3-4), 325–333 (2004).
24. D. A. Simpson, W. E. K. Gibbs, S. F. Collins, W. Blanc, B. Dussardier, G. Monnom, P. Peterka, and G. W. Baxter, "Visible and near infra-red up-conversion in Tm3+/Yb3+ co-doped silica fibers under 980 nm excitation," Opt. Express 16(18) 16, 13781–13799 (2008).
25. S. D. Jackson and S. Mossman, "Efficiency dependence on the Tm3+ and Al3+ concentrations for Tm3+-doped silica double-clad fiber lasers," Appl. Opt. **42**(15), 2702–2707 (2003).
26. S. D. Jackson and T. A. King, "Theoretical modeling of Tm-doped silica fiber lasers," J. Lightwave Technol. **17**(5), 948–956 (1999).